REPUBLIC OF AZERBAIJAN

On the rights of the manuscript

ABSTRACT

of the dissertation for the degree of Doctor of Philosophy

PHASE EQUILIBRIA IN THE $Sb_2Te_3+2BiI_3 \leftrightarrow Bi_2Te_3+2SbI_3$ AND $Bi_2S_3-BiI_3-Bi_2Te_3$ SYSTEMS, PHYSICAL AND CHEMICAL PROPERTIES OF INTERMEDIATE PHASES

Speciality:	2303.01 – Inorganic chemistry
Field of science:	Chemistry

Applicant: **Elvin Javanshir Ahmadov**

Baku – 2022

The dissertation work was carried out in the research laboratory "Thermodynamics of functional inorganic materials" of the Institute of Catalysis and Inorganic Chemistry of the Azerbaijan National Academy of Sciences.

Scientific supervisor: D. Sci. Chem., Corr.-member of ANAS
Mahammad Baba Babanly

Official opponents: D. Sci. Chem., professor
Ozbak Misirkhan Aliyev

D. Sci. Chem., professor
Yusif Amirali Yusibov

Ph. D. Chem
Guntekin Miralam Shukurova

Dissertation council ED1.15 of Supreme Attestation Commission under the President of the Republic of Azerbaijan operating at Institute of Catalysis and Inorganic Chemistry named after academician M.Nagiyev

Chairman of the Dissertation council
D. Sci. Chem., Academician
Dilgam Babir Taghiyev

Scientific secretary of the Dissertation council
Ph. D. Chem., docent
Ulviyya Akhmed Mammadova

Chairman of the scientific seminar
D. Sci. Chem., professor
Akif Shikhan Aliyev

GENERAL DESCRIPTION OF WORK

The relevance of the theme and the degree of development. The creation of new materials for various purposes with special physical properties for high-tech is one of the most pressing problems of modern chemical materials science.

Chalcogenides and chalcohalogenides of arsenic subgroup elements, as well as phases based on them, have long been in the focus of researchers as perspective functional materials including photoelectric, thermoelectric, ferroelectric, optical, etc. properties. Many of these materials are used in power converters and various fields of electronics. In recent years, interest in layered chalcogenides and chalcohalogenides of antimony and bismuth has increased sharply. This is due to fact that these phases exhibit unique physical properties, such as topological insulator (TI) and Rashba spin splitting (RSS). TI and RSS materials are very promising for application in spintronics, quantum computers, medicine, security systems, and other areas of high-tech.

The purposeful search, obtention, and design of new multicomponent chalcogenide and chalcohalogenide phases are directly related to the study of phase equilibria, thermodynamic, crystallochemical, and other physicochemical properties of relevant systems. Phase diagram allows predicting new phases in the system, to determine the nature of their formation, thermal resistance, phase transformations, primary crystallization and homogeneity areas, etc. These data also comprise the thermodynamic properties and crystallographic parameters of intermediate phases and the physicochemical basis of the directional synthesis of new materials.

One of the ways to create new materials with functional properties is obtaining solid solutions based on known compounds with appropriate properties. Because it is possible to optimize the properties of solid solutions by changing the composition at a certain range.

In recent years, four-component systems with general formulas Sb-Bi-Te-Hal $B^V - X - X' - Hal$ and $B^V - X(X') - Hal - Hal'$ (X, X' and Hal, Hal' are two different chalcogens or halogens, respectively) that possess TI and RSS properties are of great interest in terms of the search for new pnictogen, chalcogen, and halogen-subs-

tituted solid solutions based on antimony (bismuth) tellurides and tellurohalogenides. These systems are expected to form wide areas of solid solutions based on the corresponding chalcogenide, chalcohalogenide, and halogenide phases in the $Sb_2Te_3 - Bi_2Te_3 - BiHal_3 - SbHal_3$, $B_2^VX_3 - B_2^VX_3' - B^VHal_3$, $B_2^VX_3 - B^VHal_3 - B^VHal_3'$ concentration planes, respectively.

Analysis of the literature data shows that the phase equilibria on the above-mentioned concentration planes have not been studied practically until our studies. Only the Bi_2Se_3–Bi_2Te_3–BiI_3 system has been studied.

Object and subject of research. The research objects of the dissertation were $Sb_2Te_3+2BiI_3 \leftrightarrow Bi_2Te_3+2SbI_3$ and $Bi_2S_3-BiI_3-Bi_2Te_3$ systems.

The purpose and objectives of the study: The purpose of the dissertation is to obtain new reliable data on phase equilibria and thermodynamic properties in $Sb_2Te_3+2BiI_3 \leftrightarrow Bi_2Te_3+2SbI_3$ reciprocal and $Bi_2S_3-BiI_3-Bi_2Te_3$ quasi-ternary systems.

To achieve this goal, the following **specific tasks** were set and solved:

- Synthesis and physicochemical study of the $Sb_2Te_3+2BiI_3 \leftrightarrow Bi_2Te_3+2SbI_3$ and $Bi_2S_3-BiI_3-Bi_2Te_3$ systems;
- Determination of phase equilibria in these systems, construction of their liquidus surface projections, various polythermal and isothermal sections of phase diagrams, determination of types and coordinates of non- and monovariant equilibria;
- Analytical 3D modeling of phase diagrams of the $Sb_2Te_3+2BiI_3 \leftrightarrow Bi_2Te_3+2SbI_3$ and $Bi_2S_3-BiI_3-Bi_2Te_3$ systems;
- Determination of the primary crystallization and homogeneity areas of the newly revealed intermediate phases, synthesis and characterization of their selected samples;
- Investigation of thermodynamic properties of intermediate phases in the $Bi_2S_3-Bi_2Te_3-Te-S$ system;
- Investigation of $Bi_{1-x}Sb_xTeI$ solid solutions using spectroscopic ellipsometry and Raman spectroscopy.

Research methods. Research on the topic of the dissertation was carried out by the traditional physicochemical analysis methods: diffe-

rential thermal analysis (DTA), X-ray diffraction analysis (XRD), electromotive force (EMF), and scanning electron microscopy (SEM). DTA was performed on a multichannel device based on the electronic data recorder "TC-08 Thermocouple Data Logger" and "NETZS8CH 404 F1 Pegasus system" equipment. Powder diffractograms were taken on the "D2 Phaser" device of the Bruker Corporation (Germany). "Keithley 2100 6 1/2 Digit Multimeter" was used for EMF measurements. SEM analysis was done using the "JEOLJSM-7600F" device. Spectroscopic ellipsometry and Raman spectroscopy measurements were carried out using "Woolam IR-VASE rotation compensator spectroscopic ellipsometer" and "Confocal Micro – Spectrometer Nanofinder 30 (Tokyo instr., Japan)", respectively.

Main provisions for the defense.

Liquidus surface projections of $Sb_2Te_3+2BiI_3 \leftrightarrow Bi_2Te_3+2SbI_3$ and $Bi_2S_3-BiI_3-Bi_2Te_3$ systems, a number of poly- and isothermal sections of phase diagrams.

1. Newly found non- and monovariant equilibria in the phase diagrams of the studied systems, their types, and coordinates.
2. The new obtained variable composition chalcohalogenide phases, their primary crystallization, homogeneity areas, and crystallographic parameters.
3. Temperature dependence of EMF in the $Bi_2S_3-Bi_2Te_3-Te-S$ system, partial molar functions of bismuth in alloys, standard integral thermodynamic functions of revealed com-pounds, and solid solutions.

Scientific novelty.

✓ The nature of physicochemical interactions has been determined for the $Sb_2Te_3+2BiI_3 \leftrightarrow Bi_2Te_3+2SbI_3$ and $Bi_2S_3-BiI_3-Bi_2Te_3$ systems. It has been shown that the BiTeI − SbTeI, and BiTeI − BiSI sections of these systems are non-quasi-binary due to the incongruent melting of one of the starting compounds, however are stable at subsolidus. Wide areas of solid solutions based on the starting compounds in the first section, and small limited solid solution areas in the second section were found;

✓ Liquidus surface projections of $Sb_2Te_3+2BiI_3 \leftrightarrow Bi_2Te_3+2SbI_3$ and $Bi_2S_3-BiI_3-Bi_2Te_3$ systems, a number of polythermal and isothermal sections of phase diagrams were constructed, primary crystallizati-

on areas of phases from the liquid, homogeneity areas, as well as, types and coordinates of non- and monovariant equilibria were determined;

✓ Newly revealed non-stoichiometric phases with different compositions were synthesized and identified, their crystal lattice types and parameters were determined;

✓ Analytical 3D modeling of crystallization surfaces of the $Sb_2Te_3+2BiI_3 \leftrightarrow Bi_2Te_3+2SbI_3$ and $Bi_2S_3-BiI_3-Bi_2Te_3$ systems was carried out. Phase diagrams of these systems and analytical dependencies for binary boundary systems are presented in the form used by the OriginLab computer software;

✓ Based on EMF measurements, a solid-phase equilibria diagram in the $Bi_2S_3-Bi_2Te_3-Te-S$ composition region of the Bi–Te–S system at 300 K was constructed, the relative partial molar functions of bismuth in alloys of different phase areas were calculated. The thermodynamic functions of the tetradymite mineral and solid solution based on it with $Bi_2Te_{1.8}S_{1.2}$ formula were determined for the first time;

✓ Dielectric functions and Raman spectra of $Bi_{1-x}Sb_xTeI$ (x = 0; 0.05 and 0.1) phases were studied. The nature of the dependence of the dielectric function on the photon energy was identified based on the obtained ellipsometric data, while Raman spectra show that no structural changes were observed with an increasing amount of antimony in the solid solution.

The theoretical and practical significance of the work. The newly obtained results on the phase equilibria and thermodynamic properties of the $Sb_2Te_3+2BiI_3 \leftrightarrow Bi_2Te_3+2SbI_3$ and $Bi_2S_3-BiI_3-Bi_2Te_3$ systems are a contribution to the chemistry and thermodynamics of the multicomponent chalcoiodide and chalco-genide phases. These results can be used for the directional synthesis and single crystal growth methods of newly found phases in these systems. It is possible to change the composition of substitution solid solutions based on chalcoiodide compounds in a wide range, which opens up new possibilities for optimizing the properties.

The practical significance of the research is that the constructed phase diagrams, thermodynamic and crystallographic properties of the phases are fundamental physical and chemical parameters and can be included in relevant electronic databases and handbooks.

Testing and application. The results of the work were reported and discussed at the following scientific conferences: VIII Всероссийская конференция с международным участием «Физико-химические процессы в конденсированных средах и на межфазных границах - Фагран-2018» (Воронеж, Россия 2018); «5th International Turkic World Conference on Chemical Sciences and Technologies – ITWCCST-2019» (Sakarya, Türkiyə 2019); Beynəlxalq elmi konfrans «Müasir təbiət və iqtisad elmlərinin aktual problemləri» (Gəncə, Azərbaycan 2019, 2020, 2021), «1st International congress on natural sciences» (Erzurum, Türkiyə 2021).

Published scientific works: A total of 14 scientific works including 6 articles (4 articles indexed in Clarivate Analytics and Scopus databases) based on the materials of the dissertation, were published in scientific journals. 6 scientific works were published as abstracts of reports at various international conferences.

The name of the organization in which the dissertation work is carried out. The dissertation work was carried out in the "Inorganic functional materials" department of the Institute of Catalysis and Inorganic Chemistry of the Azerbaijan National Academy of Sciences.

Personal contribution of the author. Experimental research in the dissertation work, processing of the obtained results, and preparation of materials for publication was carried out mainly by the author. The author's share in the co-authorship of scientific works was decisive.

The volume and structure of the work. The dissertation consists of an introduction (9164 symbols), four chapters (I-35274, II-32819, III-40273, IV-35603 symbols), main results, a list of used scientific literature in 225 titles and has a volume of 162 pages. The thesis includes 66 figures and 25 tables.

MAIN CONTENT OF WORK

In **the introduction** part of dissertation work, the relevance of the dissertation is justified, the purpose of the work, scientific novelty, practical significance and the main provisions for defense is given.

In **the first chapter** of the dissertation, the current state of research on Bi (Sb) containing multicomponent chalcogenide and chalcohalo-genide systems was carried out and the choice of research objects

was justified.

It also provides literature data on phase equilibria and physicochemical properties in the binary and ternary boundary systems of the $Sb_2Te_3+2BiI_3 \leftrightarrow Bi_2Te_3+2SbI_3$ reciprocal and $Bi_2S_3–BiI_3–Bi_2Te_3$ quasi-ternary systems. This information was used for planning of experimental studies and the analysis of the obtained results.

The second chapter is devoted to a brief description of the synthesis and physicochemical research methods used in the dissertation.

The primary binary and ternary compounds of the studied systems were synthesized by co-melting of stoichiometric quantities of high purity (99.999%) elementary components (purchased from German company Alfa Aesar) in quartz ampoules under vacuum (~ 10^{-2} Pa). Due to the high saturated vapor pressure of sulfur and iodine at the melting temperatures of the compounds, the synthesis was carried out in an inclined two-zone furnace. The identification of the synthesized compounds was checked by DTA and XRD methods.

Samples of the studied systems were prepared by melting of pre-synthesized and identified starting binary and ternary compounds in quartz ampoules under vacuum conditions. After synthesis, the samples were subjected to short and long-term heat treatment at temperatures below 30-50 °C from the solidus, depending on the melting characteristics, and were gradually cooled by switching off the furnace from the power source. Specific synthesis conditions of compounds and samples are given in the dissertation.

The synthesized samples were characterized using DTA (TC-08 Thermocouple Data Logger and NETZSCH 404 F1 Pegasus devices; chromel-alumel thermocouples), XRD (Bruker D2 Phaser diffractometer, CuK_α-radiation) and SEM (JEOLJSM-7600F scanning electron microscopy) methods.

The third chapter presents the results of the study of phase equilibria in the $Sb_2Te_3+2BiI_3 \leftrightarrow Bi_2Te_3+2SbI_3$ and $Bi_2S_3–BiI_3–Bi_2Te_3$ systems.

Phase equilibria in the $Sb_2Te_3+2BiI_3 \leftrightarrow Bi_2Te_3+2SbI_3$ system. In order to determine the nature of the phase equilibria in this system, obtained results on a number of internal sections and the literature data of boundary quasibinary systems were processed together.

SbTeI−BiTeI section. Figure 1 presents the powder XRD patterns of thermally treated alloys. As can be seen, diffraction patterns of all the samples between pure BiTeI and the alloy of the 40 mol% BiTeI composition are similar to each other and differ only by a slight shift of the diffraction lines. On the other hand, the diffraction pattern of the 10 mol% BiTeI sample consists mainly of the SbTeI diffraction lines. The powder diffractograms of the 20 and 30 mol% BiTeI-containing samples consist of peaks of both mutually saturated solid solutions.

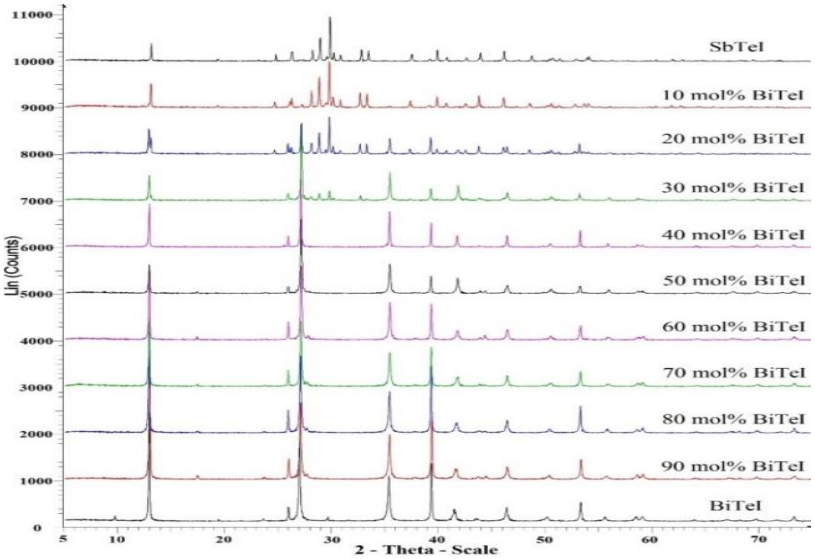

Figure 1. Powder diffractograms of some alloys of the SbTeI-BiTeI system

T-x diagram (Fig.2) of the system was constructed using DTA results. The system is completely non-quasibinary due to the incongruent melting character of the SbTeI. However, it is stable in subsolidus and forms wide substitutional solid solutions based on the starting compounds. Liquidus consists of two curves. A solid phase of $Sb_{2-x}BixTe_3$ composition (α-phase) primarily crystallizes in the 0-80 mol% BiTeI composition intervale, while solid solutions based on BiTeI (γ_2-phase) crystallize in the >80 mol% BiTeI phase region. Crystallization in the L+α field continues with monovariant $L+\alpha \leftrightarrow \gamma_1$

and L+α ↔γ_2 peritectic reactions (Fig. 6; Table1). The horizontal line at 668 K conforms L+α+γ_2↔γ_2 transition reaction. The γ_1+γ_2 phase is formed as a result of this reaction in ~ 15-27 mol% BiTeI concentration range. At the peritectic reaction temperature, the homogeneity area of the γ_1 – phase is ~ 15 mol%, and the homogeneity area of the γ_2 - phase is ~ 73 mol%.

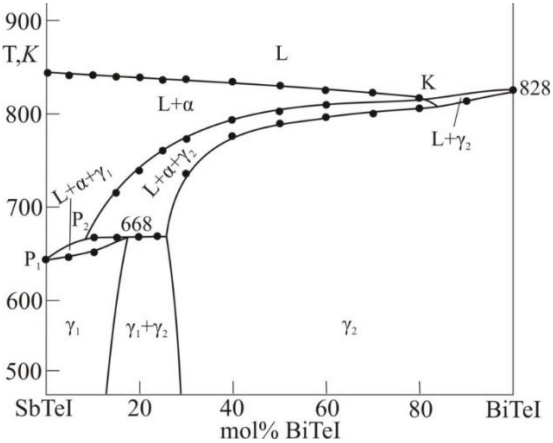

Figure 2. Phase diagram of the SbTeI-BiTeI system

Solid-phase equilibria diagram at 300K (Fig. 3). It can be seen from the phase diagram that the system is reversible reciprocal, which means it does not have a stable diagonal. This can be explained by the fact that one of the boundary quasi-binary sides of the system (Sb_2Te_3−Bi_2Te_3) forms continuous (α), the other (SbI_3−BiI_3) wide solid solution areas (β_1 and β_2) on the basis of starting binary compounds. Experience has shown that such reciprocal systems are usually adiagonal, because the decisive role in the formation of phase areas belongs to solid solutions, not stoichiometric compounds.

The SbTeI−BiTeI quasi-stable section is divided the system into two independent subsystems in the subsolidus: Sb_2Te_3−SbTeI−BiTeI−Bi_2Te_3 and SbI_3−SbTeI−BiTeI−BiI_3. These subsystems do not have a stable diagonal as well.

All phase fields shown in Fig.3 were confirmed by XRD and SEM methods. XRD patterns and SEM images of some samples (a-e) are given in Figures 4 and 5, respectively.

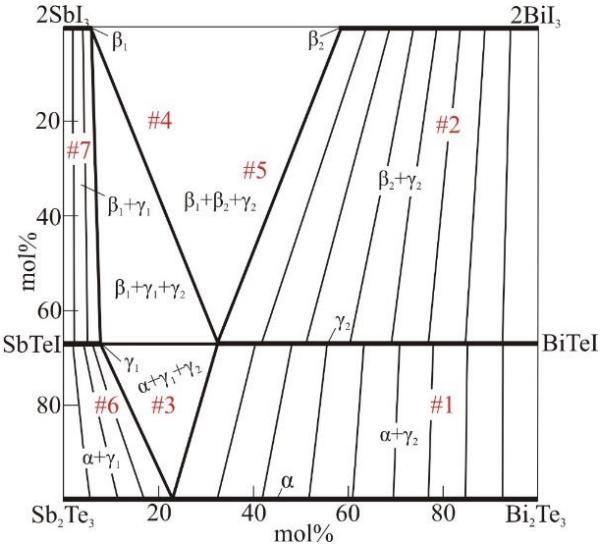

Figure 3. Solid-phase equilibria diagram of the $Sb_2Te_3+2BiI_3 \leftrightarrow Bi_2Te_3+2SbI_3$ system at 300 K

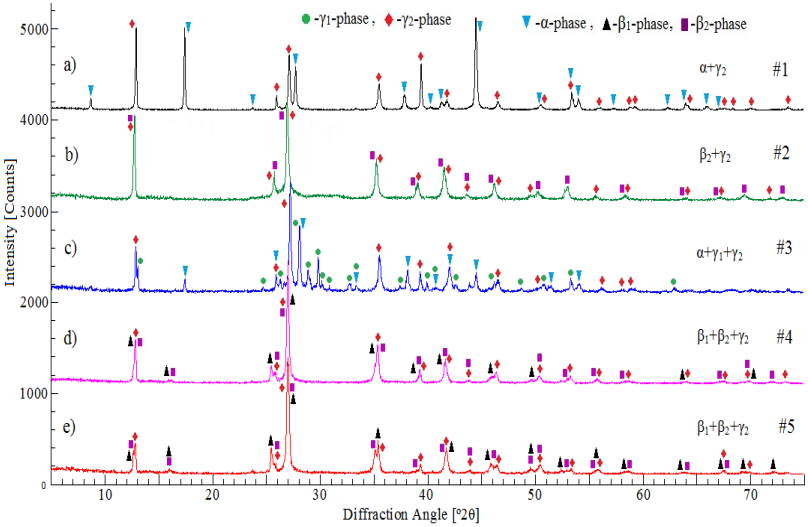

Figure 4. XRD patterns for selected alloys of the $Sb_2Te_3+2BiI_3 \leftrightarrow Bi_2Te_3+2SbI_3$ system in Fig. 3: #1 (a) $80\%Bi_2Te_3–20\%2SbI_3$; #2 (b) $20\%Sb_2Te_3–80\%2BiI_3$; #3 (c) $80\%Sb_2Te_3–20\%2BiI_3$; #4 (d) $20\%Bi_2Te_3–80\%2SbI_3$ və #5 (e) $60\%SbI_3–40\%BiTeI$

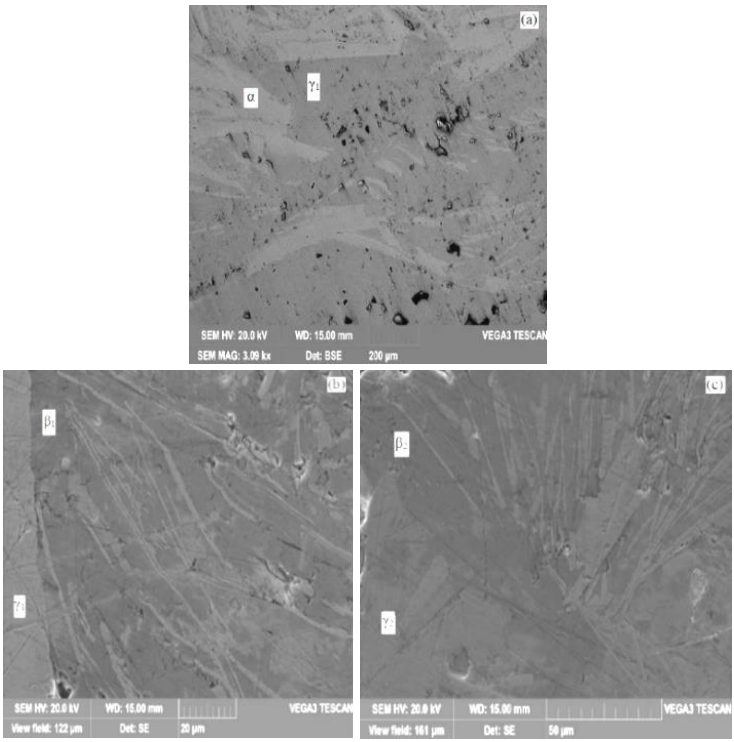

Figure 5. SEM images of some samples of the $Sb_2Te_3+2BiI_3 \leftrightarrow Bi_2Te_3+2SbI_3$ system in Figure 3:a) #6; b) #7; c) #2

The diffraction pattern of sample #1 consists of peaks of the α and γ_2 phases, and the diffraction pattern of sample #2 consists of the diffraction lines of the β_2 and γ_2 phases. The diffraction patterns of samples #3, #4, and #5 confirm that they are triphasic. Sample #3 consists of the diffraction lines of α, γ_1 and γ_2 phases, while samples #4 and #5 consists of the diffraction lines of β_1, β_2, and γ_2 phases.

In Figure 4, the diffraction lines of the different phases are marked with different colored figures. Also, the formation of $\alpha+\gamma_1$, $\beta_1+\gamma_1$ and $\beta_2+\gamma_2$ two-phase fields in the phase diagram is confirmed by the SEM results of samples # 6, # 7 and # 2 (Fig 5a-c). It is seen that γ_1-phase co-crystallizes with α-phase in Figure 5a, and with β_1-phase in Figure 5b. The two-phase equilibrium of γ_2 and β_2-phases shown in Figure 4b is confirmed by the sample # 2 in Figure 5c.

The liquidus surface projection. The liquidus surface of the system consists of 5 primary crystallization fields (Fig. 6). The widest liquidus surfaces belong to the α- and γ_2- phases (1 and 2 fields). This opens up a wide range of possibilities for the selection of liquid phase compositions for single crystals growth of given compositions by directional crystallization.

The liquidus surfaces of the other phases (β_1-, β_2- and γ_1- solid solutions) are in the form of thin strips along with the SbI_3–BiI_3 boundary system. This is due to their crystallization temperatures are very low compared to the α- and γ_2- phases

The liquidus surfaces of the different phases are separated by a series of monovariant equilibrium curves and nonvariant equilibrium points. The types of all observed nonvariant and monovariant equilibria in the system are given in Table 1. The composition and temperatures of nonvariant equilibrium points, temperature ranges of monovariant equilibrium curves are given in this Table as well.

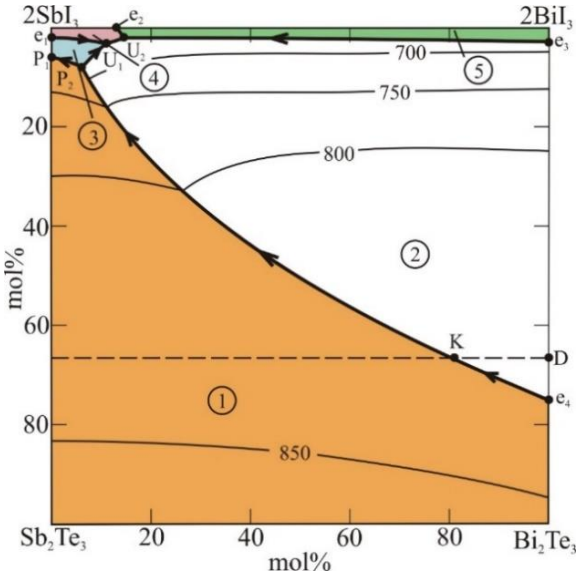

Figure 6. The liquidus surface projection of the Sb_2Te_3+2BiI_3↔Bi_2Te_3+2SbI_3 system. The primary crystallization fields of phases: 1-α; 2-γ_2; 3-γ_1; 4-β_1; 5-β_2

It should be noted that the eutectic equilibrium curve starting from the e_4-eutectic point crosses the SbTeI−BiTeI quasi-stable section and transform into a peritectic equilibrium curve on this section (Fig. 6, K-point). Therefore, this curve is shown as 2 independent curves (e_4K and KP_2) in Table 1.

Table 1

Non- and monovariant equilibria in the $Sb_2Te_3+2BiI_3 \leftrightarrow Bi_2Te_3+2SbI_3$ system

Points in Fig. 6	Equilibria	Composition, mol%			T,K
		Sb_2Te_3	Bi_2Te_3	$2SbI_3$	
D	$L \leftrightarrow BiTeI$	–	66,67	–	828
e_1	$L \leftrightarrow SbTeI + SbI_3$	1	–	99	444
e_2	$L \leftrightarrow \beta_1 + \beta_2$	–	–	87	418
e_3	$L \leftrightarrow BiTeI + BiI_3$	–	2	–	680
e_4	$L \leftrightarrow Bi_2Te_3 + BiTeI$	–	75	–	823
P_1	$L + Sb_2Te_3 \leftrightarrow SbTeI$	5	–	95	645
P_2	$L + \alpha + \gamma_2 \leftrightarrow \gamma_1$	8	–	85	668
U_1	$L + \gamma_1 \leftrightarrow \beta_1 + \gamma_2$	3	–	86	442
U_2	$L + \gamma_2 \leftrightarrow \beta_1 + \beta_2$	2	–	84	438
e_4K	$L \leftrightarrow \alpha + \gamma_2$				823-810
KP_2	$L + \alpha \leftrightarrow \gamma_2$				810-665
P_2P_1	$L + \alpha \leftrightarrow \gamma_1$				665-645
P_2U_1	$L \leftrightarrow \gamma_1 + \gamma_2$				665-442
e_1U_1	$L \leftrightarrow \beta_1 + \gamma_1$				444-442
U_1U_2	$L \leftrightarrow \beta_1 + \gamma_2$				442-438
U_2e_2	$L \leftrightarrow \beta_1 + \beta_2$				438-418
e_3U_2	$L \leftrightarrow \beta_2 + \gamma_2$				680-438

Phase equilibria in the Bi_2Te_3−Bi_2S_3−BiI_3 system.

Analysis of XRD results of samples of the **BiSI − BiTeI section** shows that it is stable in solid-state (Fig.7).

As can be seen, the diffraction pattern of a sample containing 90 mol% BiSI consists mainly of the BiSI diffraction peaks, where the most intensive peaks of BiTeI are observed at 12.8º, 26.9º, 35.5º, and 46.3º. The diffraction pattern of a sample containing 10 mol% BiSI consists mainly of diffraction peaks of BiTeI, where the most intensive peaks of solid solutions based on BiSI are observed at 18º, 20.1º, 22.5º,

and 28.5º. According to these results, it can be estimated that the homogeneity of BiTeI at room temperature is ~ 7-8 mol%, and ~ 5 mol% for BiSI. Diffraction patterns of samples containing 10-90 mol% BiSI consist of peaks of both mutually saturated solid solutions.

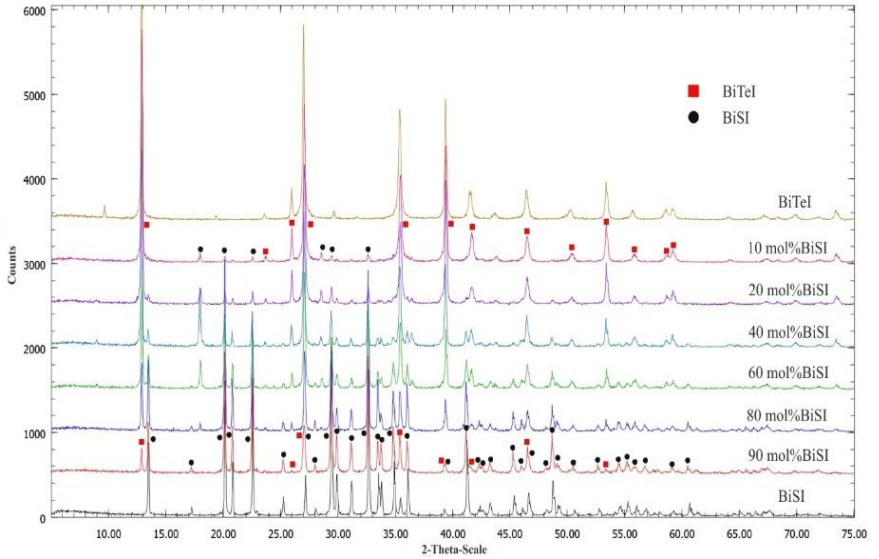

Figure 7. XRD patterns of some alloys of the BiTeI-BiSI system

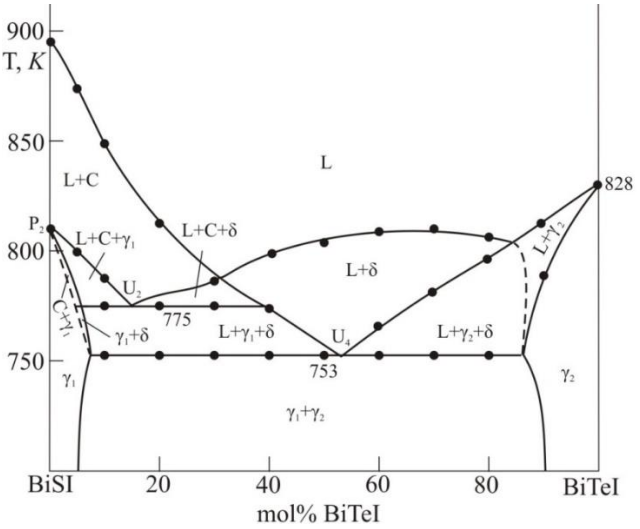

Figure 8. Phase diagram of the BiTeI-BiSI system

It is shown from the T-x diagram (Fig. 8) that the system is completely non-quasi-binary because the BiSI compound melts with the peritectic reaction, but is stable at subsolidus and forms limited solid solution fields based on the starting compounds (γ_1 and γ_2 phases).

Solid-phase equilibria diagram at 300K. Our results also confirmed the existence of β_1-, β_2- and δ- phases along the Bi_2S_3–Bi_2Te_3 boundary quasibinary system. As a result of the interaction of the above-mentioned phases and BiI_3 phase, a number of two and three-phase fields are formed in the subsolidus of the Bi_2S_3–Bi_2Te_3–BiI_3 system (Fig. 9).

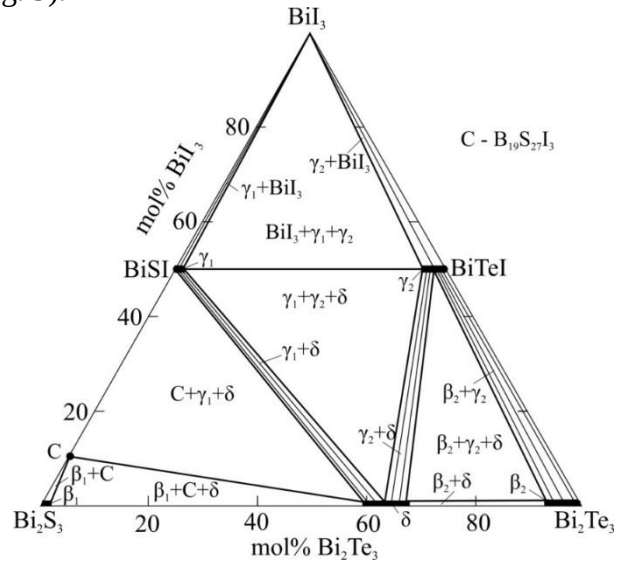

Figure 9. Solid-phase equilibria diagram of the Bi_2Te_3–Bi_2S_3–BiI_3 system at 300 K

As can be seen from Figure 9, the Bi_2S_3+3BiTeI↔Bi_2Te_3+3BiSI reciprocal system in the Bi_2S_3–BiSI–BiTeI–Bi_2Te_3 field of the concentration triangle is reversible reciprocal, and none of its diagonals is stable. In this subsystem, the decisive role in the formation of phase fields belongs to the δ-phase based on tetradymite. This phase forms stable tie-lines with all other phases (β_1 (Bi_2S_3), β_2 (Bi_2Te_3), C ($Bi_{19}S_{27}I_3$), γ_1 (BiSI), γ_2 (BiTeI)) of the subsystem: δ+β_1, δ+β_2, δ+C, δ+γ_1 və δ+γ_2.

Four three-phase fields β_1+C+δ, C+γ_1+δ, γ_1+γ_2+δ və β_2+γ_2+δ are formed between these two-phase fields, two-phase fields of side quasi-binary systems - β_1+C, C+γ_1, β_2+γ_2, as well as γ_1+γ_2 tie line.

The liquidus surface projection. Figure 10 shows types of revealed non- and monovariant equilibria in the system, while coordinates are listed in Tables 2 and 3, respectively.

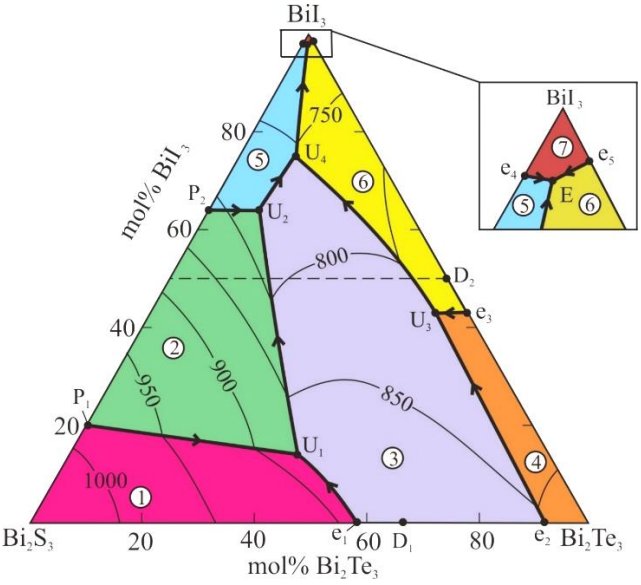

Figure 10. The liquidus surface projection of the Bi_2S_3–Bi_2Te_3–BiI_3 system. The primary crystallization fields of phases: 1-β_1, 2-$Bi_{19}S_{27}I_3$ (c), 3-δ, 4-β_2, 5-γ_1, 6-γ_2, 7-BiI_3

It can be seen in Figure 10 that the liquidus surface consists of 7 primary crystallization fields and they contain all existing phases in the system. 1-3 fields in the picture, which reflect the primary crystallization of β_1, C **(**$Bi_{19}S_{27}I_3$), and δ-phases from the liquid phase, occupy large areas in the concentration triangle. The liquidus surface of the BiI_3 compound has almost degenerated. This field is schematically zoomed in Figure 10 (scale is negligible).

Primary crystallization fields are delimited by two peritectic (P_1U_1, P_2U_2) and nine eutectics (e_1U_1, U_1U_2, e_2U_3, e_3U_3, U_2U_4, U_3U_4,

U_4E, e_4E, e_5E) equilibrium curves (Table 3). Conjugate points of all three primary crystallization surfaces represent four-phase nonvariant equilibria. Four of these points (U_1, U_2, U_3 və U_4) represent transition equilibria, and one reflects (E) eutectic equilibrium (Table 2). All these points follow "star rule".

Table 2

Nonvariant equilibria in the Bi_2S_3-Bi_2Te_3-BiI_3 system

Points in Fig. 10	Equilibria	Composition, mol%		T,K
		BiI_3	Bi_2Te_3	
D_1	$L \leftrightarrow Bi_2Te_2S$	–	66,67	898
D_2	$L \leftrightarrow BiTeI$	50	50	828
P_1	$L + \beta_1 \leftrightarrow c$	20	–	990
P_2	$L + c \leftrightarrow \gamma_1$	63	–	808
U_1	$L + \beta_1 \leftrightarrow \delta + c$	13		880
U_2	$L + c \leftrightarrow \gamma_1 + \delta$	64		775
U_3	$L + \beta_2 \leftrightarrow \gamma_2 + \delta$	43		807
U_4	$L + \delta \leftrightarrow \gamma_1 + \gamma_2$	74		753
e_1	$L \leftrightarrow \beta_1 + \beta_2$	–	59	895
e_2	$L \leftrightarrow \beta_2 + \delta$	–	91	853
e_3	$L \leftrightarrow \beta_2 + \gamma_2$	43	57	823
e_4	$L \leftrightarrow \gamma_1 + BiI_3$	97	–	670
e_5	$L \leftrightarrow \gamma_2 + BiI_3$	~99	~1	680
E	$L \leftrightarrow \gamma_1 + \gamma_2 + BiI_3$	~99	<1	668

Table 3

Monovariant equilibria in the Bi_2S_3-Bi_2Te_3-BiI_3 system

Curves in Fig. 10	Equilibria	T,K
e_1U_1	$L \leftrightarrow \beta_1 + \delta$	895-880
P_1U_1	$L + \beta_1 \leftrightarrow c$	990-880
U_1U_2	$L \leftrightarrow c + \delta$	880-775
P_2U_2	$L + c \leftrightarrow \gamma_1$	808-775
U_2U_4	$L \leftrightarrow \gamma_1 + \delta$	775-753
e_2U_3	$L \leftrightarrow \beta_2 + \delta$	853-807
e_3U_3	$L \leftrightarrow \beta_2 + \gamma_2$	823-807
U_3U_4	$L \leftrightarrow \gamma_2 + \delta$	807-753
U_4E	$L \leftrightarrow \gamma_1 + \gamma_2$	753-668
e_4E	$L \leftrightarrow \gamma_1 + BiI_3$	670-668
e_5E	$L \leftrightarrow \gamma_2 + BiI_3$	680-668

In the third chapter of the dissertation, a number of polythermal sections of both systems are given and explained in detail.

Multi 3D modeling of phase diagrams of Sb_2Te_3+BiI_3↔ Bi_2Te_3+SbI_3 and Bi_2S_3−BiI_3−Bi_2Te_3 systems. In both systems, analytical expressions were obtained for the liquidus surfaces of different phases, and using these expressions crystallization fields were modeled and their 3D images were created (Fig. 11). Analytical dependencies for crystallization surfaces were obtained using the liquidus temperatures of different samples of boundary quasi-binary and ternary systems. Analytical expressions allow to visualize crystallization surfaces separately and on one graph for all phases.

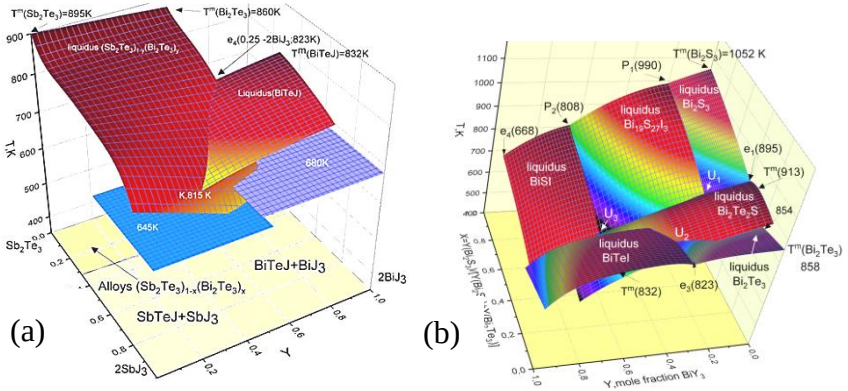

Figure 11. 3D images of crystallization surfaces of different phases in the Sb_2Te_3+2BiI_3↔Bi_2Te_3+2SbI_3 (a) and Bi_2S_3−BiI_3−Bi_2Te_3 (b) systems

The fourth chapter is dedicated to the study of the thermodynamic properties of binary and three-component phases formed in the Bi_2S_3−Bi_2Te_3−Te−S composition region of the Bi−Te−S system by electromotive force (EMF) method.

At the beginning of the chapter, the basics of the EMF method for thermodynamic study, its advantages and disadvantages are briefly explained, use of solid and liquid electrolytes is explained. Also, the specific aspects of its application to multicomponent heterogeneous systems are studied and experimental research is planned. Then, the application of EMF method and mathematical processing of results are

given. In the last two paragraphs, the results of the thermodynamic study of the intermediate phases of the Bi_2S_3–Bi_2Te_3–Te–S system are presented and discussed.

For the thermodynamic study of the Bi_2S_3–Bi_2Te_3–Te–S system, concentration cell of (1) type were assembled:

$$(-)\ Bi\ (s.)\ \big|\ \text{ionic liquid} + Bi^{3+}\ \big|\ Bi\text{-}S\text{-}Te\ (s.)\ (+) \qquad (1)$$

Elemental bismuth was used as the left electrode. The right electrodes were made from equilibrated alloys of Bi_2S_3+Te+S, Bi_2S_3+Te+γ and Bi_2Te_3+Te+γ three-phase fields and homogeneity field of γ-phase with 0.5 mol% tellurium excess (solid solution based on γ – Bi_2Te_2S).

$BiCl_3$ added ionic liquid (morpholine formate) was chosen as the electrolyte. Morpholine, formic acid, and anhydrous $BiCl_3$ (Alfa Aesar) were used to prepare the ionic liquid.

EMF measurements were performed with a Keithley 2100 6 1/2 Digit Multimeter, and results were processed using "Microsoft Excel 2010" computer program. The detailed description of the experiments is given in the dissertation.

The temperature dependencies of EMF were determined for all studied alloys. EMF values for alloys taken from Bi_2S_3+S+Te three-phase field were measured in the 300-380 K temperature range, while other alloys are measured in the 300-450 K temperature range.

Our EMF measurements showed linearity of the EMF dependences upon temperature. This indicates that the composition of the equilibrium phases in the relevant heterogeneous fields is stable regardless of temperature, and it provides a basis for thermodynamic calculations based on the EMF measurements.

The results of EMF measurements were processed by the least-squares method and presented in the form of equations:

$$E = a + bT \pm t\left[\frac{S_E^2}{n} + S_b^2(T - \overline{T})^2\right]^{1/2} \qquad (2)$$

Here n - is the number of pairs of E and T values; S_E and S_b - are dispersions of individual EMF measurements and constant b; $\overline{T}$ - the average absolute temperature; t – Student's test. In experiments where the number of test points is $n \geq 20$, at 95% confidence interval is $t \leq 2$.

In order to perform thermodynamic calculations for different phase fields, equations of (2) type were obtained (Table.4). Using these equations and

$$\Delta\bar{G}_{Bi} = -zFE$$

$$\Delta\bar{S}_{Bi} = zF\left(\frac{\partial E}{\partial T}\right)_P = zFb$$

$$\Delta\bar{H}_{Bi} = -zF\left[E - T\left(\frac{\partial E}{\partial T}\right)_P\right] = -zFa$$

thermodynamic expressions, the relative partial molar functions of bismuth in alloys were calculated (Table.5). In these expressions, z - is the charge of the potential-forming component; F - Faraday constant; a and b are constants of equation (3).

Table 4

Temperature dependences of the EMF measurements of the (1) type cells for some phase fields of the Bi_2S_3–Bi_2Te_3–Te–S system

№	Phase area	$E, mV = a + bT \pm t \cdot S_E(T)$
1	Bi_2S_3+S+Te	$359{,}58 - 0{,}0639T \pm 2\left[\frac{0{,}25}{30} + 1{,}6 \cdot 10^{-5}(T - 341{,}5)^2\right]^{1/2}$
2	Bi_2S_3+ $Bi_2Te_{1.8}S_{1.2}(\gamma)$+Te	$230{,}53 - 0{,}0347T \pm 2\left[\frac{0{,}21}{30} + 3{,}7 \cdot 10^{-6}(T - 375{,}5)^2\right]^{1/2}$
3	$Bi_2Te_2S(\gamma)$+Te	$223{,}34 - 0{,}0489T \pm 2\left[\frac{0{,}22}{30} + 3{,}9 \cdot 10^{-6}(T - 375{,}5)^2\right]^{1/2}$
4	Bi_2Te_3+γ+Te	$142{,}18 - 0{,}0266T \pm 2\left[\frac{0{,}20}{30} + 3{,}5 \cdot 10^{-6}(T - 375{,}5)^2\right]^{1/2}$

Table 5

The relative partial thermodynamic functions of bismuth in alloys of the Bi_2S_3-Bi_2Te_3-Te-S system (T=298 K)

Phase area	$-\Delta\bar{G}_{Bi}$	$-\Delta\bar{H}_{Bi}$	$\Delta\bar{S}_{Bi}$
	kJ/mol		J/(mol·K)
Bi_2S_3+S+Te	98,568±0,113	104,08±0,78	-18,50±2,28
Bi_2S_3+$Bi_2Te_{1.8}S_{1.2}(\gamma)$+Te	63,736±0,099	66,73±0,42	-10,04±1,11
$Bi_2Te_2S(\gamma)$+Te	60,428±0,102	64,65±0,43	-14,16±1,14
Bi_2Te_3+γ+Te	38,855±0,097	41,15±0,41	-7,71±1,08

According to the phase diagram, the partial molar functions of bismuth in the Bi_2S_3+S+Te and Bi_2Te_3+γ+Te three-phase fields are thermodynamic functions of the following virtual-cell reactions:

$$Bi+1.5S=0.5Bi_2S_3 \quad (3)$$

$$Bi+1.5Te=Bi_2Te_3 \quad (4)$$

The EMF values for the Bi_2S_3+$Bi_2Te_{1.8}S_{1.2}$ (γ)+Te three-phase field correspond to the virtual-cell reaction:

$$Bi + \frac{1}{3} Bi_2S_3 + 1{,}5Te = \frac{5}{6} Bi_2Te_{1.8}S_{1.2} \quad (5)$$

According to the relations (3) - (5), the standard integral thermodynamic functions and standard entropies of Bi_2S_3, Bi_2Te_3 and sulfur-rich γ-phase ($Bi_2Te_{1.8}S_{1.2}$) can be calculated by the following equations:

$$\Delta_f Z^0(Bi_2S_3) = 2\Delta\bar{Z}_{Bi} \quad (6)$$

$$\Delta_f Z^0(Bi_2Te_3) = 2\Delta\bar{Z}_{Bi} \quad (7)$$

$$\Delta_f Z^0(Bi_2Te_{1.8}S_{1.2}) = 1.2\Delta\bar{Z}_{Bi} + 0.4\Delta_f Z^0(Bi_2S_3) \quad (8)$$

$$S^0(Bi_2S_3) = 2\Delta\bar{S}_{Bi} + 2S^0(Bi) + 3S^0(S) \quad (9)$$

$$S^0(Bi_2Te_3) = 2\Delta\bar{S}_{Bi} + 2S^0(Bi) + 3S^0(Te) \quad (10)$$

$$S^0(Bi_2Te_{1.8}S_{1.2}) = 1.2\Delta\bar{S}_{Bi} + 1.2S^0(Bi) + 0.4S^0(Bi_2S_3) + 1.8S^0(Te) \quad (11)$$

In expressions (6) - (8), Z ≡ G(H).

Integral thermodynamic functions of the γ-phase corresponding to Bi_2Te_2S stoichiometric composition were calculated by graphical integration of the Gibbs-Duhem equation.

Table 6

Integral thermodynamic functions of phases in the Bi-S-Te system

Phase	$-\Delta_f G^0(298\ K)$	$-\Delta_f H^0(298\ K)$	$S^0(298\ K)$
	kJ·mol^{-1}		J·mol^{-1}·K^{-1}
Bi_2S_3	197,1±0,2	208,2±1,1	172,2±4,7
$Bi_2Te_{1.8}S_{1.2}$	155,3±0,2	163,4±0,8	214,0±2,9
Bi_2Te_2S	151,5±0,3	159,7±0,9	217,3±2,8
Bi_2Te_3	77,7±0,2	82,3±0,6	246,5±3,1

The obtained final results are given in Table 6. The standard deviations were calculated by the accumulation of errors. In addition to the data in Table 5, literature data on the standard entropies of bismuth (56,7 ± 0,5 J / (mol K)), sulfur (31,9 ± 0,2 J / (mol K)) and tellurium (49.5 ± 0.2 J / (mol K)) were used to calculate the integral thermodynamic functions.

Dielectric function and Raman spectra of $Bi_{1-x}Sb_xTeI$ solid solutions. In the dissertation, the photon energy dependence of the dielectric function which is obtained from ellipsometric data at room temperature for alloys of $Bi_{1-x}Sb_xTeI$ solid solutions with x=0; 0,05; 0,1 compositions and Raman spectra of samples of the same composition are given. The left panel of Figure 12 shows the intraband optical transitions of the bandgap at "0" crossing points of the dielectric function for $Bi_{1-x}Sb_xTeI$ solid solutions, while the right panel shows the interband optical transitions. There is no evidence that the bandgap changes depending on the composition. That is, the compositions x = 0, 0.05 and 0.1 show the same dielectric function in the region above 1 eV. This means that the intraband optical transitions in the left panel overlap with the interband optical transitions in the right panel.

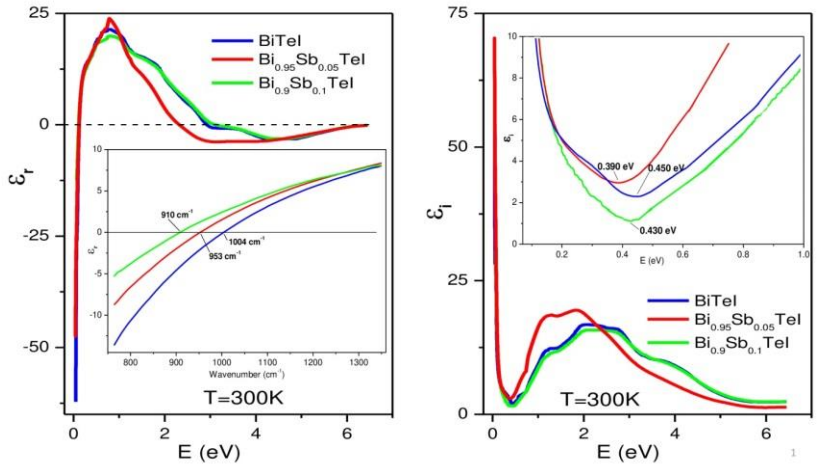

Figure 12. Dielectric function of $Bi_{1-x}Sb_xTeI$ in a wide range of photon energies: left panel-real part; right panel-imaginary part

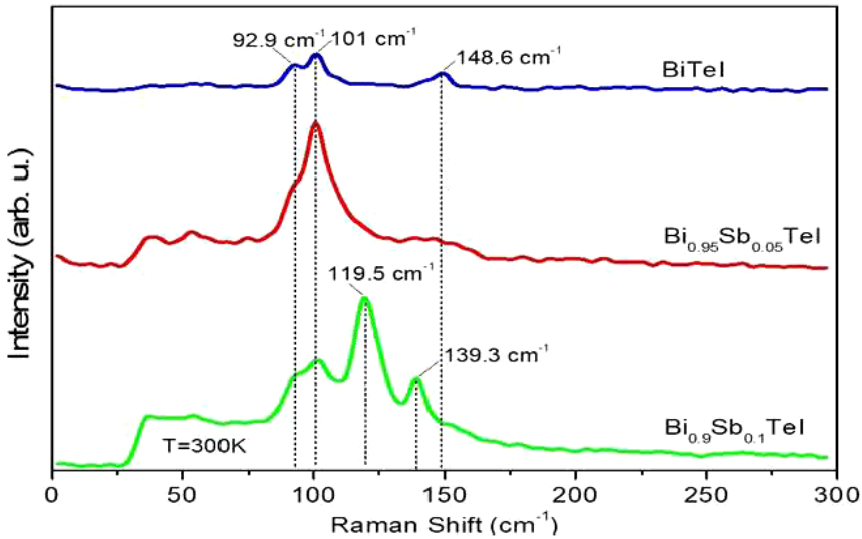

Figure 13. Raman spectra of the $Bi_{1-x}Sb_xTeI$ samples at room temperature

In Figure 13, the observed peaks with frequencies of 92.9, 101, and 148.6 cm^{-1} in the Raman curves as trilayer blocks of BiTeI are the peaks of Te, Bi, and I, respectively. Although antimony is lighter than bismuth and the atomic radius is smaller, all the effects observed in BiTeI are observed without any changes in the $Bi_{1-x}Sb_xTeI$ samples with the composition of x = 0.05 and 0.1. However, two peaks with frequencies of 119.5 and 139.3 cm^{-1} appear in the Raman spectra of a sample with x = 0.1 composition. Both peaks show strong peaks observed in the Raman spectra of pure SbTeI in the frequency range 120-140 cm^{-1}. In this case, the spectra of $Bi_{1-x}Sb_xTeI$ correspond to different crystal structures (hexagonal and monoclinic) of BiTeI and SbTeI. However, it does not indicate that the sample with x = 0.1 composition changed to the monoclinic phase. It should be noted that solid solutions between two compounds of the same structure can also show peaks of two different shapes.

Results

1. Sb-Bi-Te-I and Bi-Te-S-I systems were studied for the first time using differential thermal analysis, X-ray diffraction analysis, microstructural analysis on the $Sb_2Te_3+2BiI_3 \leftrightarrow Bi_2Te_3+2SbI_3$ and $Bi_2S_3-BiI_3-Bi_2Te_3$ concentration planes, and the nature of physical and chemical interactions were determined. It was established that these subsystems are reciprocal and quasi-ternary, respectively.
2. Liquidus surface projection of the $Sb_2Te_3+2BiI_3 \leftrightarrow Bi_2Te_3+2SbI_3$ reciprocal system, $SbTeI-BiTeI$, $2SbTeI-Bi_2Te_3$, $Sb_2Te_3-2BiTeI$, $SbTeI-BiI_3$, $SbI_3-BiTeI$, $Sb_2Te_3-2BiI_3$ polythermal sections and isothermal section at 300 K were constructed. It is shown that the liquidus surface consists of 5 primary crystallization fields. A number of mono- and nonvariant equilibria are found in the system, their types and coordinates were determined.
3. A full T-x-y diagram of $Bi_2S_3-BiI_3-Bi_2Te_3$ quasi-ternary system, $BiSI-BiTeI$, $Bi_2Te_2S-1.5BiTeI$, $1.5BiSI-Bi_2Te_3$, $Bi_2S_3-1.5BiTeI$ sections, $Bi_2Te_2S-BiI_3$ and "Bi_2Te_2S"$-BiI_3$ polythermal sections, isothermal sections at 750, 800 and 850 K were constructed. The primary crystallization areas of 7 phases, the coordinates of the curves and points that limiting them, the types of corresponding equilibria were determined.
4. It was found that the $BiTeI-SbTeI$ and $BiTeI-BiSI$ sections of the studied systems are completely non-quasi-binary due to the incongruent melting of SbTeI and BiSI compounds, but are stable at subsolidus. $BiTeI-SbTeI$ system is characterized by the formation of wide solid solution areas based on starting compounds. At room temperature, ~ 67 mol% solubility based on BiTeI and ~ 10 mol% solubility based on SbTeI were observed. In the $BiTeI - BiSI$ system, relatively small solid solution areas are formed based on starting compounds. The solubility for BiSI and BiTeI at room temperature is ~ 6 and ~ 10 mol%, respectively.
5. An analytical expression for composition dependence of primary crystallization temperatures of two- and three-component phases in the $Sb_2Te_3+2BiI_3 \rightleftarrows Bi_2Te_3+2SbI_3$ and $BiI_3-Bi_2S_3-Bi_2Te_3$ systems was determined, and three-dimensional images of liquidus surfaces

were obtained. The obtained 3D models fit well with experimentally constructed phase diagrams.

6. Based on the EMF measurements in the Bi_2S_3–Bi_2Te_3–Te–S system, the relative partial molar functions in alloys of bismuth were calculated in the relevant concentration areas. A solid-phase equilibria diagram in this composition region of the Bi-Te-S system at 300 K was constructed, standard integral thermodynamic functions of tetradymite mineral and $Bi_2Te_{1.8}S_{1.2}$ solid solution based on it, as well as Bi_2S_3 and Bi_2Te_3 compounds, were determined.
7. Raman spectra and dielectric functions of $Bi_{1-x}Sb_xTeI$ solid solutions were studied. It was found that there was no change in the structure of solid solutions up to the sample with x = 0.1 and that the interband optical transitions in the bandgap of solid solutions is overlapping with intraband transitions.

The main results of the dissertation were published in the following scientific works:

1. Ахмедов Э.Дж., Алиев З.С., Салимов З.Э., Бабанлы М.Б. Взаимная система $Sb_2Te_3+2BiI_3 \leftrightarrow Bi_2Te_3+2SbI_3$ / VIII Всероссийская конференция с международным участием «Физико-химические процессы в конденсированных средах и на межфазных границах - Фагран-2018» - Воронеж, - 2018, с. 397.
2. Ahmadov E.J., Babanly D.M., Aliyev Z.S., Babanly M.B. Phase equilibria in the system SbTeI-BiTeI // New Materials, Compounds and Applications, - 2019, 3(2), - p. 87-93.
3. Ahmadov E.J., Aliyev Z.S., Salimov Z.E., Babanly M.B. Solid-Phase Equilibria in the Bi_2S_3-BiI_3-Bi_2Te_3 Ternary System / 5th International Turkic World Conference on Chemical Sciences and Technologies – ITWCCST - Sakarya, Turkey, - 2019, s. 109.
4. Əhmədov E.C., Sultanova S.Q., Babanlı K.N., Bulanova M.V. SbTeI-BiTeI sistemində yeni dəyişən tərkibli fazalar / "Müasir təbiət və iqtisad elmlərinin aktual problemləri" beynəlxalq elmi konfrans – Gəncə, Azərbaycan, - 2019, - s. 15-17.
5. Ahmadov E.J. Physico-chemical interaction in the BiSI–BiTeI system // Azerbaijan Chemical Journal, - 2020, №1, - p. 36-40.

6. Ahmadov E.J. Physico-chemical interaction in the SbTeI–Bi_2Te_3 system // Azerbaijan Chemical Journal, - 2020, №3, - p. 46-49.
7. Əhmədov E.C., Əliyev Z.S., Babanlı M.B. Bi_2Te_2S və BiTeI birləşmələri arasinda fiziki-kimyəvi qarşiliqli təsir / "Müasir təbiət və iqtisad elmlərinin aktual problemləri" beynəlxalq elmi konfrans – Gəncə, Azərbaycan, - 2020, - s. 8-10.
8. Ahmadov E.J., Babanly D.M., Imamaliyeva S.Z., Tagiev D.B., Babanly M.B. Thermodynamic Properties of the Chalcogenide Phases in the Bi–Te–S System // Inorganic Materials, - 2021, 57(3), - p. 227-233.
9. Ahmadov E.J., Aliev Z.S., Babanly D.M., Imamaliyeva S.Z., Gasymov V.A., Babanly M.B. The Quasi-Ternary System Bi_2S_3–Bi_2Te_3–BiI_3 // Russian Journal of Inorganic Chemistry, - 2021, 66(4), - p. 538–549.
10. Ahmadov E.J., Mammadov A.N., Guliyeva S.A., Babanly M.B. Modeling of phase diagram of the system BiI_3-Bi_2S_3-Bi_2Te_3 // New Materials, Compounds and Applications, - 2021, 5(1), - p. 5-11.
11. Əhmədov E.C., Əliyev Z.S., Mahmudova M.A., Babanlı M.B. $Sb_2Te_3+2BiI_3 \leftrightarrow Bi_2Te_3+2SbI_3$ qarşılıqlı sisteminin likvidus səthinin proyeksiyası / "Müasir təbiət və iqtisad elmlərinin aktual problemləri" beynəlxalq elmi konfrans – Gəncə, Azərbaycan, - 2021, - s. 32-35.
12. Ahmadov E.J., Aliev Z.S., Babanly M.B. New variable composition phases in Sb-Bi-Te-I and Bi-Te-S-I systems / "1st International congress on natural sciences" - Erzurum, Turkey, - 2021, p.116.

The defense will be held on “21” april 2022 at 10^{00} at the meeting of the Dissertation council ED1.15 of Supreme Attestation Commission under the President of the Republic of Azerbaijan operating at Institute of Catalysis and Inorganic Chemistry named after academician M.Naghiyev.

Address: H.Cavid, 113, AZ-1143, Baku, Azerbaijan

The dissertation is accessible at the Library of Institute of Catalysis and Inorganic Chemistry named after academician M.Naghiyev.

Electronic versions of dissertation and its abstract are available on the official website of the Institute of Catalysis and Inorganic Chemistry named after academician M.Naghiyev.

Abstract was sent to the required addresses on “18” march 2022.

Signed for print: 10.03.2022

Paper format: 60x84$^{1/16}$

Volume: 37 953 characters

Number of hard copies: 20